

Zhang, H., Wu, L., Zhang, Y., An, S., Miras, H.N. and Song, Y.-F. (2020) Heteropolyacids and sulfonic acid-bifunctionalized organosilica spheres for efficient manufacture of cellulose acetate propionate with high viscosity. *Cellulose*. 27(5), pp. 2437-2453.
(doi: [10.1007/s10570-019-02936-6](https://doi.org/10.1007/s10570-019-02936-6))

The material cannot be used for any other purpose without further permission of the publisher and is for private use only.

There may be differences between this version and the published version. You are advised to consult the publisher's version if you wish to cite from it.

<http://eprints.gla.ac.uk/217029/>

Deposited on 05 June 2020

Enlighten – Research publications by members of the University of
Glasgow

<http://eprints.gla.ac.uk>

Heteropolyacids and sulfonic acid-bifunctionalized organosilica spheres for efficient manufacture of cellulose acetate propionate with high viscosity

Huaiying Zhang^a, Lifu Wu^a, Yanfen Zhang^a, Sai An^{*a}, Haralampos N. Miras^{*b}, Yu-Fei Song^{*a}

^aState Key Laboratory of Chemical Resource Engineering, Beijing Advanced Innovation Center for Soft Matter Science and Engineering, Beijing University of Chemical Technology, Beijing 100029 P. R. China.

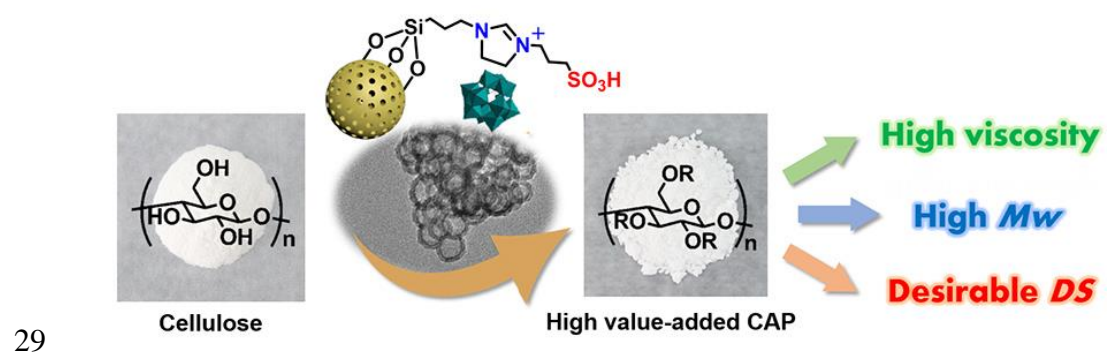
*E-mail: songyf@mail.buct.edu.cn; Fax/Tel: +86 10-64431832.

^bWestCHEM, School of Chemistry, University of Glasgow, Glasgow, G12 8QQ, UK.

Abstract. Cellulose acetate propionate (CAP), a high value-added chemical, is traditionally prepared using H₂SO₄ as catalyst. Replacement of the mineral acids by solid acids is current research focus for green and sustainable production of CAP. Herein, we reported the fabrication of novel solid acid catalyst HPW/Si(Et)Si-Dim-SO₃H (Si(Et)Si = ethyl-bridged organosilica and Dim = dihydroimidazole) by incorporating phosphotungstic acid (HPW) and sulfonic acid-based Brønsted acidic ionic liquids (BILs) onto the organosilica nanospheres of the designed catalyst for efficient manufacture CAP *via* esterification. The results indicated that the as-prepared HPW/Si(Et)Si-Dim-SO₃H with 7.5% HPW loading showed the best catalytic performance at 45 °C in 3 h and the resulting CAP exhibited viscosity of 447 mPa·s, *M_w* of 102882 and *DS* of 2.69. Most importantly, the HPW/Si(Et)Si-Dim-SO₃H exhibited high catalytic stability over six consecutive cycles and the obtained products were stable too with similar *DS*, *M_w* and viscosity. As such, the designed heteropolyacids (HPAs) and sulfonic acid-bifunctionalized heterogeneous catalyst is highly promising for biomass conversion under mild conditions.

Keywords: Solid acid catalyst, Heteropolyacids, Cellulose acetate propionate, High viscosity

28 **Graphic abstract**



30 Introduction

31 Utilization of biorenewable and biodegradable resource on earth, especially
32 cellulose, which can be considered as an inexhaustible polymeric material with
33 fascinating structure and properties, has attracted great attention due to the
34 declining fossil fuel reserves, energy and materials security, and global climate
35 change (Klemm *et al.* 2005; Chen *et al.* 2018; Su *et al.* 2014). Cellulose can be
36 used as a chemical raw material to produce various important cellulose derivatives
37 by esterification, hydrolysis, etherification *etc.* (Heinze *et al.* 2001). One
38 interesting option is the acid-catalyzed esterification of cellulose to produce
39 cellulose acetate propionate (CAP), in which some hydroxyl groups are
40 substituted with acetyl and propionyl groups. Comparing with cellulose acetate
41 (CA), CAP maintains the advantages of excellent transparency and strength, and
42 the incorporation of propionyl groups endows CAP with the properties of water
43 resistance, solubility and compatibility with other polymers. CAP, especially that
44 with high viscosity is considered as high value-added chemicals for specialty
45 coatings, plastic products, tool handles, separation membranes *etc.* (Edgar *et al.*
46 2001; Li *et al.* 2012). Therefore, the parameters such as the degree of substitution
47 (*DS*), molecular weight (*M_w*), viscosity *etc.* are the important features for
48 evaluating the performance of cellulose esterification, rather than that of
49 traditional conversion or selectivity or yield. For practical purposes, the viscosity
50 and *M_w* of CAP even should be more concerned compared to *DS*. Indeed, H₂SO₄
51 can effectively catalyze cellulose esterification. Nevertheless, such process suffers
52 from severe corrosion, cellulose degradation and decomposition and
53 uncontrollable process problems (Yan *et al.* 2009). As such, it is imperative to
54 develop environmentally benign catalytic process for cellulose esterification. To
55 date, considerable efforts have been paid and various solvents systems and
56 heterogeneous catalysts were applied for the cellulose esterification. According to
57 the reported work, the explored solvents systems can be beneficial to the
58 dissolution of cellulose such as *N,N'*-dimethylacetamide/LiCl (El Seoud *et al.*
59 2000; Marson *et al.* 1999), 4-methylmorpholine-*N*-oxide (Biganska *et al.* 2005),
60 tetrabutylammonium fluoride trihydrate/DMSO (Heinze *et al.* 2000; Hussain *et al.*
61 2004) and ionic liquids (Barthel *et al.* 2006; Huang *et al.* 2011; Köhler *et al.* 2007;
62 Wu *et al.* 2004; Abbott *et al.* 2005; Cao *et al.* 2007, 2009). Besides, several
63 sulfated metal oxides like SO₄²⁻/ZrO₂ (Yan *et al.* 2006) and SO₄²⁻/TiO₂ (Meng *et*

64 *al.* 2017) were employed for the synthesis of cellulose ester due to their strong
65 acidity. However, the industrial processing and practical applications of CAP is
66 greatly restricted by these catalytic systems because it is really challenging to
67 obtain the CAP with high viscosity and M_w *etc.*

68 Heteropolyacids (HPAs) are a class of discrete anionic metal oxides with
69 attractive properties (Song *et al.* 2012; Omwoma *et al.* 2014; An *et al.* 2019).
70 They have been regarded as the potential green alternatives to traditional mineral
71 acids owing to their tunable Brønsted or Lewis acidity, thermal stability, redox
72 properties, *etc.* (Tao *et al.* 2015, 2017; Li *et al.* 2016; Shi *et al.* 2017; Li *et al.*
73 2017; Zhang *et al.* 2019; Fan *et al.* 2013). For instance, cellulose acetate with DS
74 of *ca.* 2.2 can be obtained by phosphotungstic acid-catalyzed esterification of
75 cellulose with acetic anhydride in dichloromethane (Fan *et al.* 2013). However, it
76 is still a high challenge in extensive application of HPAs due to the problems of
77 their low BET surface areas ($< 10 \text{ m}^2 \text{ g}^{-1}$), difficult recovery and separation.
78 Tightening environmental legislation is driving the chemical industries to
79 manufacture high value-added CAP by developing efficient and environmental-
80 benign solid acid catalyst.

81 Under such circumstances, aiming at development of green and sustainable
82 cellulose esterification process, we herein reported a series of heterogeneous
83 catalysts by immobilizing HPW and sulfonic acid-based BILs on organosilica
84 nanospheres (donated as HPW/Si(Et)Si-Dim-SO₃H). The as-prepared
85 HPW/Si(Et)Si-Dim-SO₃H exhibited much higher viscosity and M_w compared
86 with H₂SO₄ *etc.* under the same reaction.

87 **Experimental section**

88 **Chemical and reagents.** 1,2-Bis(trimethoxysilyl)ethane (BTMSE, 97%),
89 Pluronic P123 (EO₂₀PO₇₀EO₂₀) and Pluronic F127 (EO₁₀₆PO₇₀EO₁₀₆) were
90 purchased from Sigma-Aldrich Company Ltd. 1,3,5-trimethylbenzene (TMB) was
91 obtained from Tianjin Guangfu Fine Chemical Research Institute. *N*-[3-
92 (triethoxysilyl)propyl]-4,5-dihydroimidazole (98%) and 1,3-propanesultone (98%)
93 were purchased from Sigma-Aldrich. Phosphotungstic acid (HPW),
94 phosphomolybdic acid (HPMo), silicotungstic acid (HSiW) and silicomolybdic
95 acid (HSiMo) were purchased from Tianjin Fuchen Chemical Reagent Factory.

96 Ethanol, toluene, acetone, hydrochloric acid, acetic acid and propionic acid were
97 obtained from Beijing Chemical Works. Acetic anhydride and propionic
98 anhydride were purchased from Sinopharm Chemical Reagent Co., Ltd., and
99 microcrystalline cellulose was obtained from Alfa Aesar.

100 All chemicals were analytical reagent grade. Anhydrous toluene was
101 obtained by treating toluene with sodium, and the other chemicals were directly
102 used without purification.

103 **Preparation of HPW/Si(Et)Si-Dim-SO₃H.** The synthesized method of
104 mesoporous organosilica nanospheres was referenced to the literature (An *et al.*
105 2016). Typically, P123 (0.25 g), F127 (0.10 g), HCl (2.20 mL), and TMB (0.70
106 mL) were successively added into deionized water (12.90 mL) with stirring at
107 room temperature for 2 h. After heated to 40 °C, BTMSE (0.61 mL) was added
108 dropwise into the mixture and pre-hydrolyzed for 45 min. Then, *N*-[3-
109 (triethoxysilyl)propyl]-4,5-dihydroimidazole (0.14 mL) was added to the mixture
110 with stirring for 24 h and aged at 100 °C for another 24 h. The obtained
111 suspension was separated by filtration and drying. Then, the solid was dispersed
112 in ethanol (50 mL) and refluxed at 80 °C for 6 h for three times and drying
113 overnight to remove the template. Subsequently, the obtained solid was dispersed
114 with 1,3-propanesultone (0.27 mL) in anhydrous toluene (30 mL) and refluxed at
115 80 °C for 24 h. The solid named Si(Et)Si-Dim⁺-SO₃⁻ was obtained followed by
116 separation, washing with ethanol and acetone and drying. Finally, the as-prepared
117 Si(Et)Si-Dim⁺-SO₃⁻ and HPW (0.085 g) were added into deionized water (50 mL)
118 with stirring at room temperature for 12 h. HPW/Si(Et)Si-Dim-SO₃H was
119 successfully fabricated followed by separation, washing with water and drying.

120 **Preparation of HPAs/Si(Et)Si-Dim-SO₃H.** In order to investigate the
121 influence of the composition of Keggin type HPAs on catalytic performance, we
122 prepared HPMo/Si(Et)Si-Dim-SO₃H, HSiW/Si(Et)Si-Dim-SO₃H and
123 HSiMo/Si(Et)Si-Dim-SO₃H by a similar procedure as the above HPW/Si(Et)Si-
124 Dim-SO₃H except that HPMo, HSiW and HSiMo were used instead of HPW.

125 **Preparation of HPW/Si(Et)Si-Dim-SO₃H-3D_{int}.** In order to investigate the
126 influence of the morphological characteristics on catalytic performance, the
127 counterpart with 3D interconnected mesostructure (HPW/Si(Et)Si-Dim-SO₃H-
128 3D_{int}) was prepared by a similar procedure as the above HPW/Si(Et)Si-Dim-SO₃H
129 except the molar ratio of composition. The molar ratio of P123 : HCl : BTMSE :

130 N -[3-(triethoxysilyl)propyl]-4,5-dihydroimidazole : 1,3-propanesultone : HPW =
 131 86 : 3600 : 2409 : 520 : 3054 : 30.

132 **Catalytic tests.** The esterification of cellulose to synthesis CAP was carried
 133 out in a round-bottom flask in a temperature-controlled oil bath. As shown in
 134 Scheme 1, the procedure for esterification of cellulose (2 g, 12.5 mmol) to
 135 synthesis CAP suffered from activation by acetic acid (10 g, 167 mmol) and
 136 propionic acid (10 g, 135 mmol) at room temperature for 1 h firstly. Then, the
 137 esterifying agent acetic anhydride (10 g, 100 mmol) and propionic anhydride (10
 138 g, 75 mmol) were added consecutively into the activated cellulose, followed by
 139 the as-prepared catalyst (25 mg). The reaction mixture was keeping in stirring at
 140 45 °C for 3 h to complete the esterification. Subsequently, the reaction mixture
 141 was centrifuged and filtered to obtain viscous CAP solution and recovered
 142 catalyst. Finally, the CAP was gradually precipitated by dropping the above
 143 viscous liquid into 5-fold deionized water and was collected followed by filtering,
 144 washing and drying overnight.

145 For the study of reusability and the characterization of used-catalyst after
 146 each catalytic cycle, the separated catalyst powder was collected by washing with
 147 acetone and deionized water and drying overnight, followed by using in another
 148 catalytic cycle.



150 **Scheme 1** Illustration for the procedure of esterification of cellulose to CAP

151 The degree of substitution (DS) of CAP were determined by ^1H NMR spectra
 152 at room temperature. The samples were dissolved in CDCl_3 , containing a drop of
 153 deuterated trifluoroacetic acid to shift active hydrogen to low field area. The DS
 154 of CAP was calculated using the following equations according to the literature
 155 method: (Huang *et al.* 2011)

$$DS_A = \frac{I_A \times 7}{I_{AGU} \times 3} \quad (1)$$

$$DS_P = \frac{I_P \times 7}{I_{AGU} \times 3} \quad (2)$$

$$DS_{total} = DS_A + DS_P \quad (3)$$

$$A\% = \frac{DS_A \times 43}{162 - DS_{total} + DS_A \times 43 + DS_P \times 57} \times 100\% \quad (4)$$

$$P\% = \frac{DS_P \times 57}{162 - DS_{total} + DS_A \times 43 + DS_P \times 57} \times 100\% \quad (5)$$

where DS_A , DS_P , and DS_{total} are the degree of substitution of acetyl, propionyl and total acyl groups, respectively. I_A , I_P , and I_{AGU} are the peak integrals of the methyl protons of the acetyl (δ 2.0, 3H) and propionyl (δ 1.0, 3H), and all protons of the anhydroglucose unit (AGU) (δ 2.8–5.9, 7H), respectively.

For viscosity measurement, 2.0 g of CAP was added into acetone (8.0 g) to dissolve the sample. The viscosity was determined in water-bath at 25 °C.

Characterization. Transmission electron microscopy (TEM) and high-resolution transmission electron microscopy (HRTEM) observations were performed on a Hitachi H-800 instrument and a JEOL JEM-2010 electron microscope operating at 400 kV, respectively. The N₂ adsorption-desorption measurements were performed on a Micromeritics ASAP 2020M surface area and porosity analyzer after the samples were degassed under vacuum at 100 °C for 6 h before measurements. Fourier transform infrared (FT-IR) spectra were collected on a Bruker Vector 22 infrared spectrometer using the KBr pellet method. X-ray photoelectron spectroscopy (XPS) measurements were recorded with monochromatized ALK exciting X-radiation (PHI Quantera SXM). The solid-state NMR experiments were performed on a Bruker Avance 300M solid-state spectrometer equipped with a commercial 5 mm MAS NMR probe. Thermogravimetric (TG) analysis was tested by an STA-449C Jupiter (HCT-2 Corporation, China) under air atmosphere (20 mL min⁻¹) with a heating rate of 10 °C min⁻¹. HPW loading was determined by inductively coupled plasma atomic emission spectroscopy (ICP-AES) analysis that carried out on a Shimadzu ICPS-7500 instrument. The acid concentrations were tested by acid-base titration. The initial electrode potential (E_i) was determined by SNR B639073181 (Mettler Toledo), with DGi115-SG electrode. ¹H and ¹³C NMR spectra of the CAP were

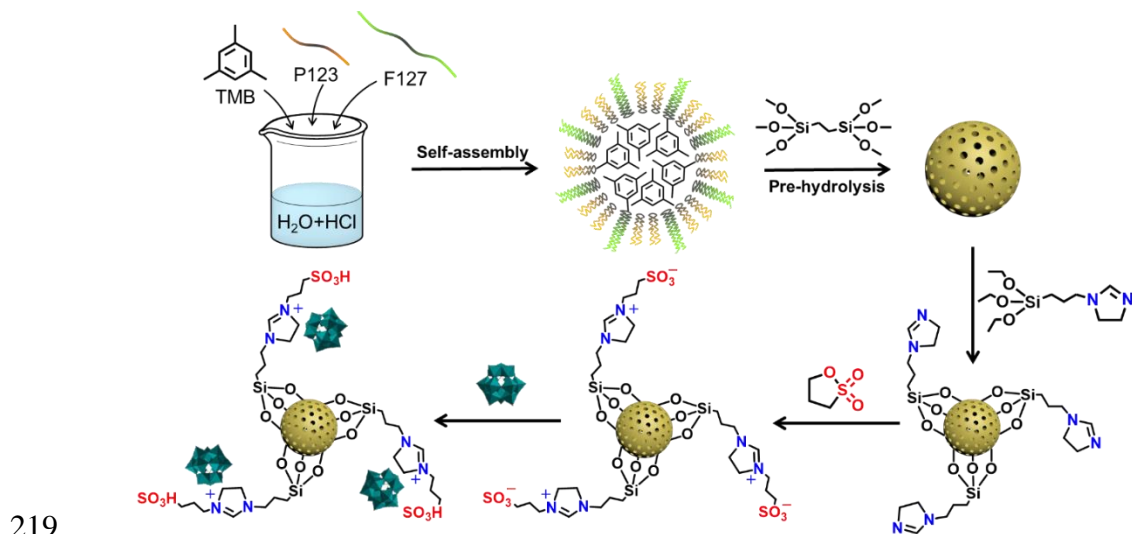
186 collected on a Bruker AV400 NMR spectrometer at 400 MHz. Heteronuclear
187 singular quantum (HSQC) and heteronuclear multiple bond correlation (HMBC)
188 2D NMR spectra were acquired on a Bruker AV600 NMR spectrometer at 600
189 MHz. The M_w of CAP were determined by Gel permeation chromatography
190 (GPC) analysis, which was performed with 515 HPLC pump and 2410 RI
191 Detector (Waters Corporation, America) with tetrahydrofuran as the mobile phase.
192 The dynamic viscosity of CAP was measured with the NDJ-79 type of rotating
193 viscometer (Shanghai Changji Geological Instrument Co., Ltd).

194 **Result and discussion**

195 *Preparation of catalysts.* Taking the advantages of controllable
196 morphological nanostructure, excellent surface physicochemical properties and
197 functional diversity of organosilica (Zhang *et al.* 2014; Hu *et al.* 2011; Song *et al.*
198 2016), we fabricated organosilica-based nanospheres to provide large surface area
199 for incorporating more exposed acid sites. Moreover, the introduced sulfonic acid-
200 based BILs was contributed to increase compatibility and accessibility between
201 catalysts and substrates, and the incorporation of HPW is beneficial for the
202 controllable esterification process, which was expected to facilitate the
203 esterification.

204 The procedure for preparation of the HPAs and sulfonic acid-
205 bifunctionalized organosilica nanospheres (HPAs/Si(Et)Si-Dim-SO₃H) is shown
206 in Scheme 2, which can be divided into three processes including formation of
207 micelles, co-hydrolysis and -condensation of precursors as well as immobilization
208 of active species. During the first process, the micelles of the triblock copolymer
209 surfactant self-assembled to form spherical topography by using TMB as
210 expansion agent through hydrophilic-hydrophobic interactions. The hydrophobic
211 $-\text{CH}_2(\text{CH}_3)\text{CHO}$ blocks aggregated with hydrophobic TMB together to form a
212 core, while the hydrophilic $-\text{CH}_2\text{CH}_2\text{O}$ blocks are closed to water molecule to
213 formed the hydrated corona. Subsequently, the silica/carbon frameworks
214 gradually formed and the dihydroimidazole modified on organosilica through the
215 co-hydrolysis and co-condensation (An *et al.* 2016). For the immobilization of
216 active species, HPW was successfully incorporated by the strong electrostatic

217 interaction between anion of HPW and N^+ of the zwitterionic structure (N^+-
 218 $(CH_3)_3-SO_3^-$).



220 **Scheme 2** Illustration of the employed synthetic procedure for the preparation of HPW/Si(Et)Si-
 221 Dim-SO₃H

222 **Chemical structure.** The structural integrity of the as-prepared
 223 HPW/Si(Et)Si-Dim-SO₃H catalysts were confirmed by FT-IR (Figure 1a), W 4f
 224 XPS (Figure 1b), ³¹P (Figure 1c) and ²⁹Si MAS NMR (Figure 1d).

225 As shown in FT-IR spectra (Figure 1a), HPW/Si(Et)Si-Dim-SO₃H and
 226 Si(Et)Si exhibit the characteristic bands at 1024, 1107 and 2930 cm⁻¹, which
 227 could be assigned to the stretch vibrations of Si-O, Si-C and C-H bond of -CH₂-
 228 CH₂- group, respectively (Zhu *et al.* 2011). It is indicated that the FT-IR spectrum
 229 of HPW/Si(Et)Si-Dim-SO₃H has the characteristic S-O vibrations at 610 and 530
 230 cm⁻¹, respectively, indicating the existence of -SO₃H group (Cao *et al.* 2018).
 231 Moreover, H₃PW₁₂O₄₀ shows the characteristic vibration at 1079, 985, 890 and
 232 795 cm⁻¹, respectively, which can be assigned to the stretching of tetrahedral P-O
 233 bonds, terminal W=O_t bonds and two types of bending vibrations originating from
 234 the bridging W-O_b-W bonds (Schnee *et al.* 2017). The above characteristic
 235 vibrational signals can be observed in the FT-IR spectra of HPW/Si(Et)Si-Dim-
 236 SO₃H. The above results indicate that 1) the bridged ethyl organosilica, sulfonic
 237 acid-based BILs and HPW were successfully incorporated onto the nanospheres;
 238 2) the primary Keggin structure remained intact after immobilization.

239 In the W 4f XPS spectrum of HPW/Si(Et)Si-Dim-SO₃H (Figure 1b), it can be
 240 deconvoluted into two signals centered at 37.7 and 35.6 eV due to the W 4f_{5/2} and
 241 W 4f_{7/2} spin-orbit components accordingly (Geng *et al.* 2018). As can be seen

from the ^{31}P MAS NMR spectrum (Figure 1c), the sharp peak centered at -15.2 ppm can be assigned to the resonance of the encapsulated PO_4^{3-} units within the $\text{H}_3\text{PW}_{12}\text{O}_{40}$ cage, indicating the structural integrity of the incorporated $\text{H}_3\text{PW}_{12}\text{O}_{40}$ (Kozhevnikov *et al.* 1996). Another peak at -13.2 ppm indicates the presence of $(\equiv\text{SiOH}^{2+})(\text{H}_2\text{PW}_{12}\text{O}_{40}^-)$ species, which comes from the interaction between HPW and the $-\text{OH}$ groups of silica/carbon framework (Kozhevnikov *et al.* 1996; Lefebvre 1992; Kasztelan *et al.* 1990).

As shown in Figure 1d, the ^{29}Si MAS NMR spectrum displays two peaks corresponding to T^3 ($\delta = -64.7$ ppm) and T^2 ($\delta = -58.4$ ppm), where $\text{T}^m = \text{RSi}(\text{OSi})_m(\text{OH})_{3-m}$ ($m = 1-3$). Most importantly, there are no signals corresponding to the Q^n species, where $\text{Q}^n = \text{Si}(\text{OSi})_n(\text{OH})_{4-n}$, ($n = 2-4$), confirming that the integrity of silica/carbon framework (Inagaki *et al.* 1999, 2002).

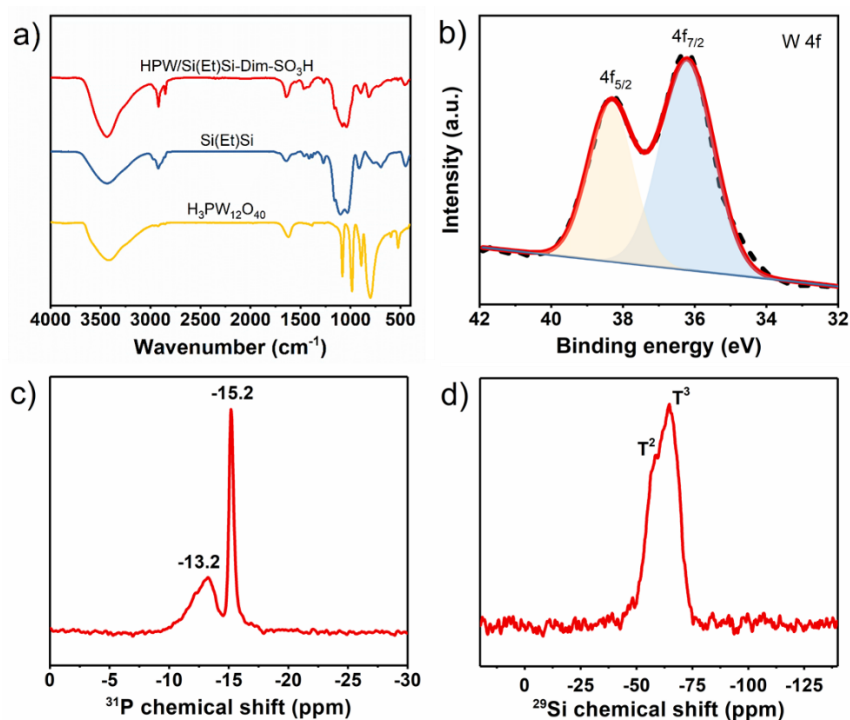


Figure 1 FT-IR spectra of HPW/Si(Et)Si-Dim-SO₃H, Si(Et)Si and H₃PW₁₂O₄₀ (a); XPS spectrum for the W 4f core level (b), ^{31}P (c) and ^{29}Si (d) MAS NMR of HPW/Si(Et)Si-Dim-SO₃H

The thermogravimetric studies were carried out in the range of 30 to 800 °C. As shown in Figure S1, the TG-DTA plot of HPW/Si(Et)Si-Dim-SO₃H shows two consecutive weight losses. The first weight loss occurs in the range of 30 to 100 °C (*ca.* 3.84%) which can be attributed to the loss of water molecules adsorbed by the catalysts. Another weight loss in the range of 200 to 600 °C (*ca.* 19.58%) can be attributed to the decomposition of the bridging ethyl groups, sulfonic acid-

based BILs, residual P123, F127 and the collapse of the silica/carbon framework and decomposition of the Keggin structure.

Based on the above structural information, we successfully fabricated the HPAs and sulfonic acid-bifunctionalized organosilica nanospheres and they are stable below 200 °C.

Morphology, porosity and acidity. TEM images of as-prepared catalysts (Figure 2) indicates that they are composed of well-dispersed nanospheres with uniform particle size. It shows that the particle size and inner diameter of HPW/Si(Et)Si-Dim-SO₃H are *ca.* 32 nm and *ca.* 17 nm, respectively, and the shell thickness is *ca.* 7 nm (Figure 2a). Comparing with Si(Et)Si-Dim-SO₃H, HPW/Si(Et)Si-Dim-SO₃H **1** and HPW/Si(Et)Si-Dim-SO₃H **2** (Figure S2), which possess different HPW loading, the spherical nanostructure is still remained, indicating that nanospheres formed by P123- and F127-directed route is stable enough. From HRTEM images of HPW/Si(Et)Si-Dim-SO₃H (Figure 2b and 2c), we can clearly see complete and well-defined nanospheres with uniformly dispersed black spots of 1–2 nm, which is in agreement with the dimensions of the H₃PW₁₂O₄₀ clusters (yellow circles in Figure 2c). Furthermore, Figure 2d shows the EDS isotherm of HPW/Si(Et)Si-Dim-SO₃H, which confirms the presence of HPW. The above results suggest that the HPW were successfully incorporated to the silica/carbon framework.

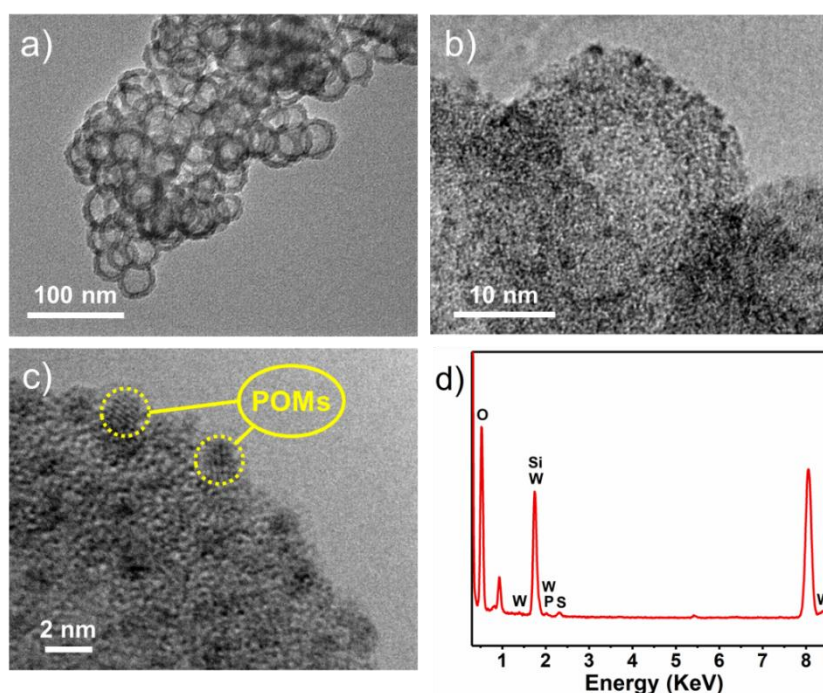


Figure 2 TEM images (a), HRTEM images (b, c) and EDS isotherm (d) of HPW/Si(Et)Si-Dim-SO₃H

Figure 3a shows the N₂ adsorption-desorption isotherms, in which the type IV isotherm confirms the mesoporous nature of the HPW/Si(Et)Si-Dim-SO₃H and Si(Et)Si. Moreover, both of them exhibit one hysteresis loop that can be attributed to the hollow interior of the spherical nanostructures or the void space formed between the loosely packed spheres. The capillary condensation steps occur at $P/P_0 = 0.45\text{--}0.99$. As shown in Figure 3b, BJH pore size distribution curves show that the HPW/Si(Et)Si-Dim-SO₃H and Si(Et)Si exhibit one peak at 15.6 nm and 15.8 nm, respectively, which confirms the mesoporous structure of the nanospheres and corresponds to the uniform hollow interior of the nanospheres.

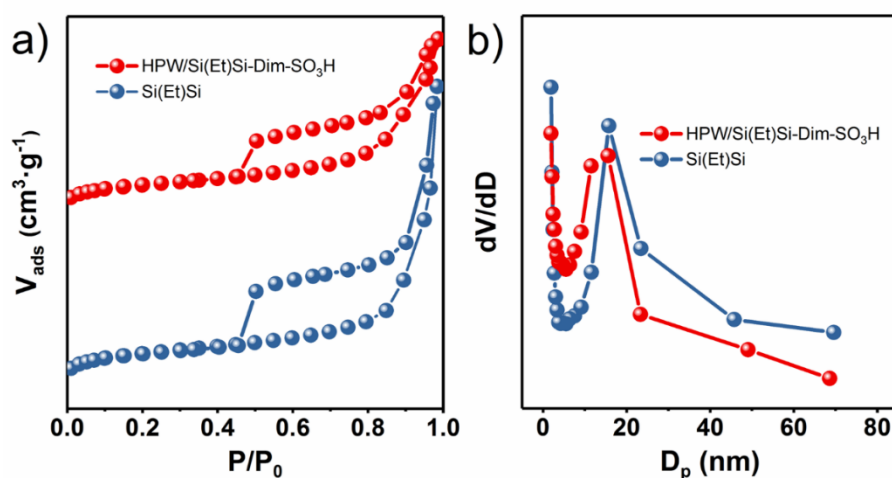


Figure 3 Nitrogen gas adsorption-desorption isotherms (a) and BJH pore size distribution profiles (b) of Si(Et)Si and HPW/Si(Et)Si-Dim-SO₃H

From the detailed textural parameters in Table 1, it can be found that as-prepared catalysts possess similar pore size (15.6 and 15.8 nm), large BET surface area (376 and 439 m² g⁻¹) and pore volume (1.11 and 1.95 cm³ g⁻¹). The as-prepared HPW/Si(Et)Si-Dim-SO₃H exhibits the acid density of 953 μmol g⁻¹. The initial electrode potential (E_i) indicates the maximum acid strength of the surface site. Materials with E_i values higher than 100 mV are defined as very strong solid acids, and that in the range of 0–100 mV can be defined as strong solid acids (Kuzminska *et al.* 2014). It can be seen that HPW/Si(Et)Si-Dim-SO₃H presents 187.7 mV of E_i , which clearly indicates that it possesses strong Brønsted acidity.

Table 1 Porosity and acidity of HPW/Si(Et)Si-Dim-SO₃H and Si(Et)Si

Catalysts	S_{BET} (m ² g ⁻¹)	D_p (nm)	V_p (cm ³ g ⁻¹)	Acid density (μmol g ⁻¹)	E_i (mV)
HPW/Si(Et)Si-Dim-SO ₃ H	376	15.6	1.11	953	187.7

Catalytic studies. In order to screen out the HPAs and sulfonic acid-bifunctionalized organosilica nanospheres with the best performance, the influences of the composition and loading of HPAs on the catalytic activity were carefully investigated. The corresponding characteristic results are displayed in Figure S1–S4.

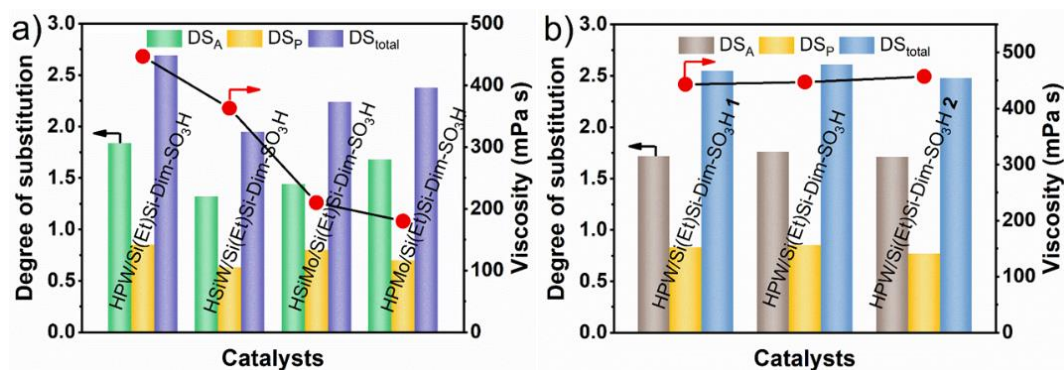


Figure 4 Influence of the composition (a) and loading (b) of HPAs on the DS and viscosity of CAP. Reaction conditions: 45 °C, 1.25 wt% catalyst, anhydride/cellulose mass ratio of 10:1 and acetic anhydride/propionic anhydride mass ratio of 1 : 1 for 3 h

The Brønsted acid strength of HPAs is closely related to the composition and the Brønsted acid strength order as follows $H_3PW_{12}O_{40} > H_3PMo_{12}O_{40} > H_4SiW_{12}O_{40} > H_4SiMo_{12}O_{40}$. Therefore, the influence of the composition of Keggin type HPAs on esterification performance was investigated firstly (Figure 4a and Table S1). Among the HPW/Si(Et)Et-Dim-SO₃H, HPMo/Si(Et)Et-Dim-SO₃H, HSiW/Si(Et)Et-Dim-SO₃H and HSiMo/Si(Et)Et-Dim-SO₃H catalysts, the highest DS of 2.69, M_w of 102882 and viscosity of 447 mPa·s are obtained by HPW/Si(Et)Et-Dim-SO₃H-catalyzed esterification reaction because of the inherent strong acidic strength of HPW. The above results further demonstrate the importance of Brønsted acid strength to the manufacture of CAP with high viscosity.

Subsequently, the influence of HPW loading on CAP properties was evaluated by choosing HPW/Si(Et)Et-Dim-SO₃H **1** (HPW loading of 5.9%), HPW/Si(Et)Et-Dim-SO₃H (HPW loading of 7.5%) and HPW/Si(Et)Et-Dim-SO₃H **2** (HPW loading of 14.2%) as representative catalysts. The results in Figure 4b and Table S1 show that DS and M_w of CAP slightly increase with increasing the HPW loading, while it decreases with further increasing the HPW loading. Meanwhile, the three products exhibit similar viscosity (ca. 443–457 mPa·s).

Based on the above results, the *DS* and *M_w* of CAP strongly linked to the HPW loading and HPW/Si(Et)Et-Dim-SO₃H-catalyzed esterification exhibit the highest *DS* (2.69) and *M_w* (102882). Therefore, HPW/Si(Et)Si-Dim-SO₃H with HPW loading of 7.5% is chosen for subsequent catalytic test.

Considering of the importance of various reaction parameters for high value-added CAP, we carefully investigated the influence of mass ratio and molar ratio of substrates, mass ratio and molar ratio of anhydride, temperature and reaction time on *DS*, viscosity and *M_w* of CAP by choosing the optimized HPW/Si(Et)Si-Dim-SO₃H as the representative catalyst.

First of all, the amount of esterifying agent (acetic anhydride and propionic anhydride), which is crucial to the properties of CAP, were studied. In Figure 5a and Table S2, the *DS*, viscosity and *M_w* gradually increased with increasing anhydride/cellulose mass ratio from 6 : 1 to 10 : 1 (molar ratio from 8.4 : 1 to 14 : 1), and the highest *DS* of 2.69, viscosity of 447 mPa·s and *M_w* of 102882 are obtained. Nevertheless, further increase of the anhydride/cellulose mass ratio to 12 : 1 (molar ratio of 16.8 : 1) and 14 : 1 (molar ratio of 19.6 : 1) leads to the decrease of *DS*, viscosity and *M_w*. Based on the principle of chemical equilibrium, higher anhydride-to-cellulose mass ratio or excessive esterifying agent can drive the equilibrium to the CAP product and thereby higher *DS* and *M_w*. However, much more esterifying agent may dilute the reaction system, leading to the poor properties of CAP. As a result, we select the anhydride and cellulose mass ratio of 10 : 1 (molar ratio of 14 : 1) for the subsequent catalytic tests.

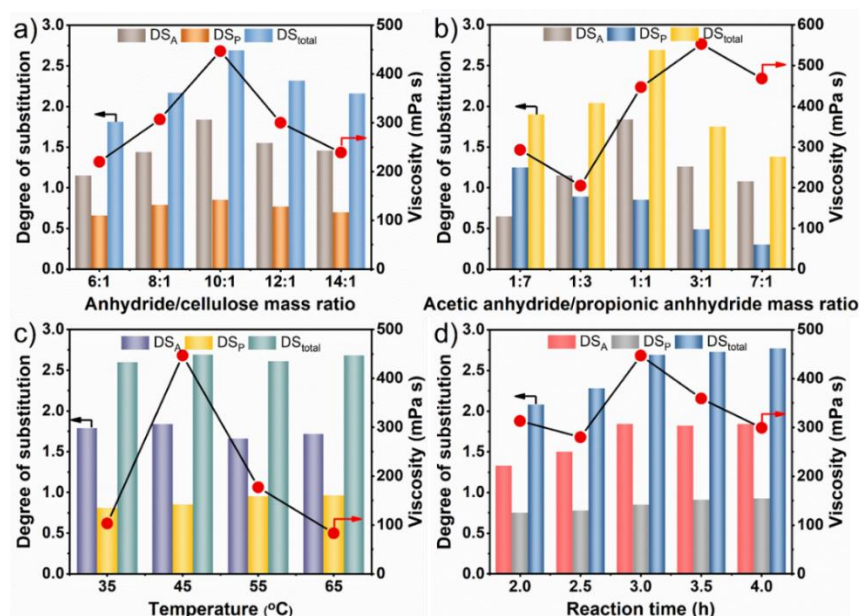


Figure 5 Influence of anhydride/cellulose mass ratio (a), acetic anhydride/propionic anhydride mass ratio (b), temperature (c) and reaction time (d) on the *DS* and viscosity of CAP

Secondly, we controlled acetic anhydride-to-propionic anhydride mass ratio to investigate the corresponding *DS*, *M_w* and viscosity of CAP (Figure 5a and Table S3). It is found that the CAP exhibits desired *DS*, high *M_w* and viscosity only under the acetic anhydride-to-propionic anhydride of 1 : 1 (molar ratio of 4 : 3). Moreover, as shown in Figure 5b, the viscosity of CAP is on the increase with *DS_P* decreasing, indicating that the content of propionyl groups has a profound influence on the CAP viscosity. Considering of *DS*, *M_w* and viscosity, 1 : 1 of acetic anhydride-to-propionic anhydride (molar ratio of 4 : 3) is selected for the subsequent catalytic tests.

Figure 5c shows the effect of reaction temperature (35, 45, 55 and 65 °C) on *DS* and viscosity of CAP. It is found that there is little difference to the *DS* (2.65–2.69) of CAP with adjusting reaction temperature because of the equilibrium of esterification of cellulose over 45 °C. However, the viscosity highly depends on the reaction temperature. For example, viscosity rises sharply from 103 to 447 mPa·s with the reaction temperature changed from 35 °C to 45 °C. Then, with further increasing reaction temperature to 55 and 65 °C, viscosity drops to 177 and 83 mPa·s, respectively. Additionally, the *M_w* of the products exhibits a similar trend with viscosity (Table S4), and exhibit the highest value of 102882 at 45 °C. This is due to that the glycosidic bonds among cellulose base rings are unstable under high temperature, leading to the degradation of cellulose. Thus, 45 °C was selected for the optimized reaction temperature.

At last, in order to investigate the influence of reaction time on catalytic performance, 2.0, 2.5, 3.0, 3.5, and 4.0 h was selected. As shown in Figure 5c, the *DS* of CAP increases obviously from 2.08 to 2.69 with prolonging reaction time from 2.0 to 3.0 h. Then, it tends to be stable when further prolonging reaction time to 3.5 and 4.0 h. On the other hand, the viscosity shows a rising trend from 2 h to 3 h and drops down to 299 mPa·s with further prolonging time to 4.0 h. This is due to the degradation of long chain in the amorphous cellulose or in the crystalline cellulose with weak intermolecular and intramolecular hydrogen bond under high temperature and acidic system.

On the basis of the above results, the optimized reaction conditions can be determined as following: 10 g acetic anhydride (100 mmol), 10 g propionic

anhydride (75 mmol), with 1.25 wt% catalyst, 45 °C, 3 h for esterification of cellulose to CAP.

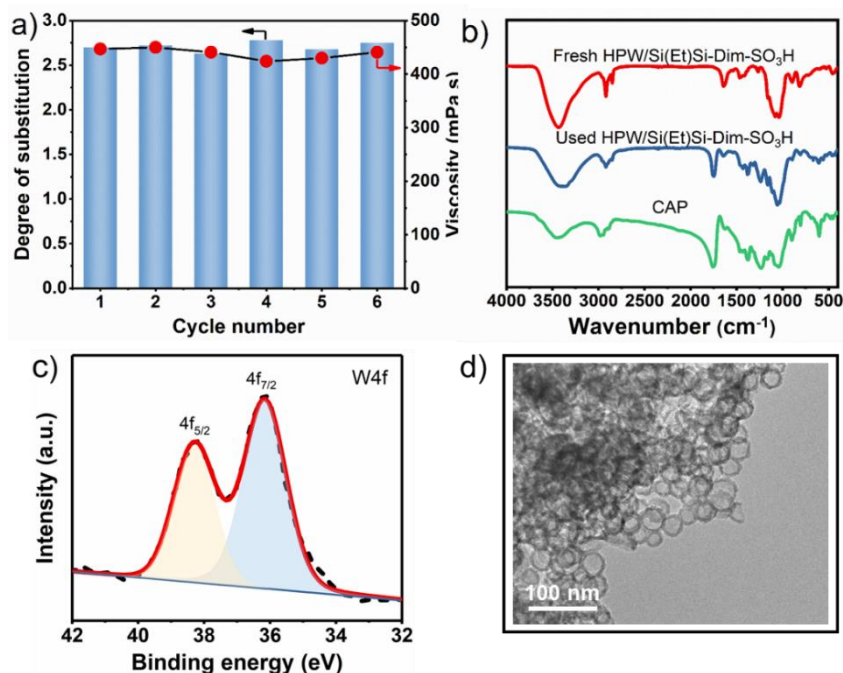


Figure 6 Reusability (a), FT-IR spectra (b), XPS spectrum of W 4f (c) and TEM image (d) of used HPW/Si(Et)Si-Dim-SO₃H

To evaluate the reusability and stability of the catalytic system, the HPW/Si(Et)Si-Dim-SO₃H catalyze the esterification of cellulose for six consecutive cycles under the optimized reaction condition. After each catalytic cycle, the separated catalyst powder was washed with acetone and deionized water and dried overnight. The details of regenerating treatment of catalysts are shown in Scheme 1. As shown in Figure 6a, the DS, *M_w* and viscosity of CAP remain the range of 2.63–2.75, 81634–91530 and 424–450 mPa·s, respectively, after six cycles. In order to identify potential leaching of the HPW into the solution, we conducted ICP-AES analysis to determine the tungsten content of reaction mixture after removing the catalyst at the end of the cycle. The results showed that the concentration of the tungsten in the system is below the detection limit, confirming that there is no detectable leaching of HPW species under this experimental condition. Subsequently, the structure of the used HPW/Si(Et)Si-Dim-SO₃H catalyst was further analyzed. In Figure 6b, the characteristic peaks assigned to the Keggin type HPW and sulfonic acid groups can be still be detected. Additionally, a new peak appears at the spectra of used HPW/Si(Et)Si-Dim-SO₃H, which attributed to the adsorption of CAP on the surface of catalysts. The deconvoluted W 4f XPS spectrum reveals again in this case two signals

centered at 38.3 and 36.2 eV (Figure 6c), originating from the contributions of the W $4f_{5/2}$ and W $4f_{7/2}$ spin-orbit components, which found to be similar to the freshly prepared HPW/Si(Et)Si-Dim-SO₃H catalyst. Additionally, TEM image (Figure 6d) exhibits well-defined hollow nanospheres, which indicates that the spherical nanostructure of as-prepared catalysts is retained after recycling. Therefore, the as-prepared HPW/Si(Et)Si-Dim-SO₃H can act as efficient and stable solid acid catalysts with excellent catalytic performance for the esterification reaction of cellulose to yield CAP at least six cycles.

Table 2 Esterification activity and CAP parameters comparison of HPW/Si(Et)Si-Dim-SO₃H with respect to commercial and reference catalysts^a

Entry	Catalyst	Time (h)	Temp. (°C)	DS_{total}	DS_A	DS_P	M_w	Viscosity (mPa·s)
1	HPW/Si(Et)Si-Dim-SO ₃ H	3	45	2.69	1.84	0.85	102882	447
2	HPW/Si(Et)Si-Dim-SO ₃ H-3D _{int}	3	45	2.77	1.91	0.86	91427	298
3	H ₂ SO ₄	3	45	2.97	2.14	0.83	82606	160
4	HPW ^b	3	45	2.58	1.82	0.76	89255	200
5	Amberlyst-15	3	45	2.79	1.99	0.80	103023	237
6	Blank	3	45	—	—	—	—	—
7	PDVB-VBC-IM-PW ₁₂ (Zhang <i>et al.</i> 2019)	3	45	2.77	1.84	0.93	92500	335
8	AmimCl (Huang <i>et al.</i> 2011)	5	100	2.67	0.21	2.46	—	—
9	Iodine (Cheng <i>et al.</i> 2011)	24	100	2.80	1.60	1.20	—	—
10	DBU/CO ₂ /DMSO (Xu <i>et al.</i> 2018)	2	80	2.72	1.76	0.96	—	—
11	TBAA (Yu <i>et al.</i> 2016)	6 ^c	65	2.99	1.79	1.20	—	—

Note: PDVB-VBC (copolymer of divinylbenzene with 4-vinylbenzyl chloride); AminiCl (1-allyl-3-methylimidazolium chloride); DBU (1, 8-Diazabicyclo[5.4.0]undec-7-ene); TBAA (tetrabutylammonium acetate). ^aReaction conditions: 2 g cellulose, 25 mg catalyst, 10 g acetic anhydride, 10 g propionic anhydride for entry 1-7; ^bEquivalent to the weight of HPW on HPW/Si(Et)Si-Dim-SO₃H; ^cAcetic anhydride was added into the reaction system 3 h after propionic anhydride.

Comparing with 3D interconnected mesostructural HPW/Si(Et)Si-Dim-SO₃H-3D_{int} (Table 2, entry 2), spherical HPW/Si(Et)Si-Dim-SO₃H exhibited higher M_w (102882) and viscosity (447 mPa s) by a controllable and mild process, which benefited from the large surface with more exposed and accessible acid sites. Furthermore, the prepared HPW/Si(Et)Si-Dim-SO₃H was compared with inorganic acid H₂SO₄, HPW and commercial available Amberlyst-15 under the same reaction conditions (Table 2, entry 3–5). As shown in entry 3 of Table 2, H₂SO₄-catalyzed cellulose esterification performed with considerably fast reaction rate, and the highest DS of 2.97, the lowest M_w (82606) and viscosity (160 mPa s)

440 were obtained, which is attributed to the degradation and decomposition of
441 cellulose. As for the others, HPW/Si(Et)Si-Dim-SO₃H obtained CAP with the
442 highest viscosity (447 mPa·s) despite their similar desired *DS* (2.58–2.79) and *M_w*
443 (89255–103023). Moreover, in the absence of any catalysts (Table 2, entry 6),
444 substrate cellulose didn't react with esterifying agent and there is no product CAP
445 can be obtained in the system after completely reaction. Comparing with our
446 previous work (Table 2, entry 7), CAP obtained by HPW/Si(Et)Si-Dim-SO₃H not
447 only maintains excellent properties but also exhibits higher *M_w* (102882),
448 viscosity (447 mPa s) and more controllable esterification process. As shown in
449 entry 8–11 of Table 2, the reported homogeneous system of cellulose
450 esterification always proceed under higher temperature (65–100 °C) or even much
451 longer reaction time (*e.g.* 24 h by iodine) than this work. It is worth noting that the
452 HPW/Si(Et)Si-Dim-SO₃H-catalyzed esterification is more controllable to keep *DS*
453 of CAP within 2.4–2.7, which meets the industrial requirements. More
454 importantly, the *M_w* and viscosity are not mentioned in most of reported work,
455 which are the crucial properties of CAP to evaluate whether they are high value-
456 added chemicals. As a consequence, as-prepared HPW/Si(Et)Si-Dim-SO₃H
457 catalyst is competitive in the esterification of cellulose to yield CAP due to the
458 excellent catalytic activity with desired *DS*, high *M_w* and viscosity under mild
459 reaction conditions.

460 ***Studies of CAP products.*** The products obtained by HPW/Si(Et)Si-Dim-
461 SO₃H-catalyzed esterification of cellulose were further characterized by ¹H, ¹³C
462 NMR spectroscopy (Figure 7a, 7b), HSQC and HMBC 2D NMR spectroscopy
463 (Figure 7c, 7d). As shown in ¹H NMR spectrum of CAP, the peaks at 3.45–5.20
464 ppm are assigned to the anhydroglucose protons. The peaks at 1.01–1.20 ppm and
465 2.16–2.44 ppm are attributed to the methyl and methylene groups of propionyl
466 moieties, respectively. Additionally, the signals assigned to methyl of acetyl are
467 observed at 1.88–2.15 ppm (Huang *et al.* 2011). In Figure 7b, the ¹³C NMR
468 spectrum of the CAP shows signals at 173 and 170 ppm, which are assigned to the
469 carbonyl carbon of propionyl and acetyl groups, respectively. The characteristic
470 signals are attributed to C1, C4, C5, C3, C2 and C6 of anhydroglucose carbonate
471 region appear at 100.5, 76.1, 72.9, 72.5, 71.8 and 62.0 ppm, respectively (Huang
472 *et al.* 2011). The peaks corresponding to the methyl and methylene groups in
473 propionyl can be observed at 9.0 and 27.3 ppm, while the peak centered at 20.4

474 ppm is assigned to methyl of acetyl. The HSQC spectrum (Figure 7c) shows the
 475 connectivity of C–H bond except for the quaternary carbons (C=O of acetyl and
 476 propionyl groups). Furthermore, the HMBC spectrum exhibits the correlations
 477 between protons of anhydroglucose and carbonyl carbons of acyl. The correlation
 478 peaks centered at 4.82×173 ppm, 4.78×170 ppm, 5.10×173 ppm and 5.06×170
 479 ppm confirm that the acetyl and propionyl groups are mostly substituted at C2 and
 480 C3.

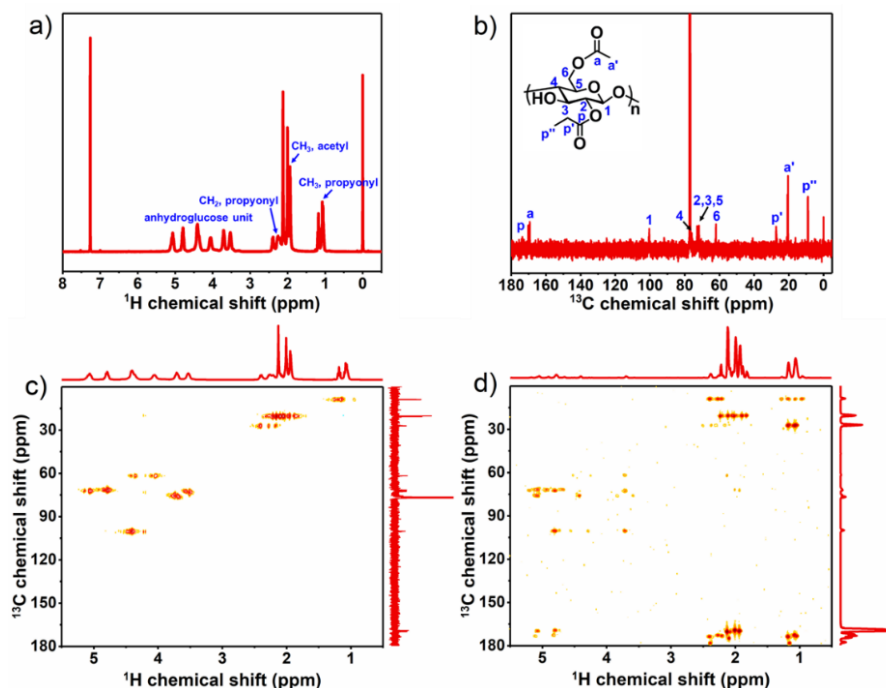
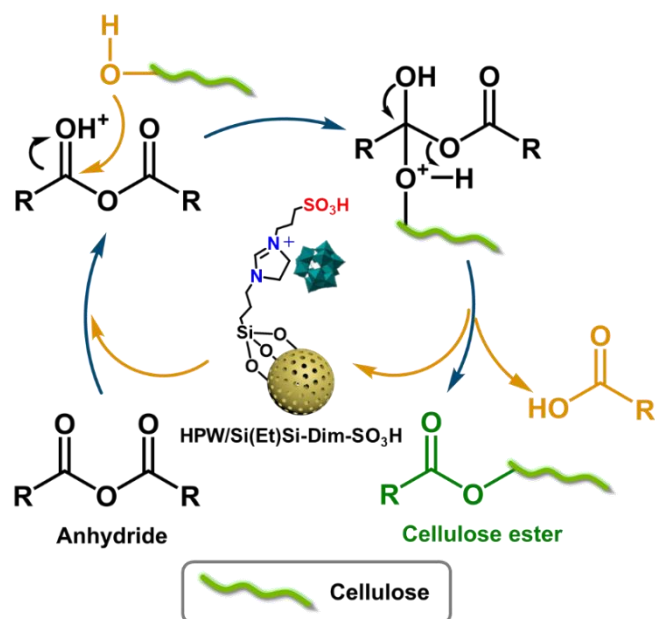


Figure 7 ^1H NMR (a), ^{13}C NMR (b) spectra, HSQC (c) and HMBC (d) 2D NMR spectra of CAP

Furthermore, the thermogravimetric studies were carried out in the range of
 30 to 600 °C. As shown in Figure S5, the TG-DTA plots show only one weight
 loss at 367.9 °C for CAP obtained by HPW/Si(Et)Si-Dim-SO₃H-catalyzed
 cellulose esterification and 334.4 °C for cellulose. It can be seen that it is a rapid
 decomposition process due to the breakage of intermolecular glycoside and C–C
 bonds with increasing temperature. Comparing with cellulose, the thermostability
 of CAP was obviously enhanced due to the incorporation of acetyl and propionyl
 groups.



Scheme 3 The proposed mechanism of HPW/Si(Et)Si-Dim-SO₃H-catalyzed cellulose esterification

Mechanism. For a typical manufacturing process of CAP, it concludes three parts of cellulose activation, cellulose esterification and separation with catalysts. The strong intermolecular and intramolecular hydrogen bonds presented in cellulose are conducive to forming crystalline regions, hindering small solvent molecules from contacting with the cellulose molecules and thereby reducing the solubility (Yu *et al.* 2016; Wu *et al.* 2004). Therefore, the activation of cellulose is an important step in a typical esterification reaction of cellulose to synthesize CAP. During the process of activation, the crystallinity of cellulose decreased and the structure of amorphous and outermost cellulose was destroyed after the infiltrating of acetic acid and propionic acid. Meanwhile, the accessibility of hydroxyl was improved due to the breakage of the hydrogen bonds between cellulose molecules. It is worth noting that the activation process is a physical swelling process to change the crystalline of cellulose, which not occurs chemical reaction.

Taking the HPW/Si(Et)Si-Dim-SO₃H-catalyzed esterification process as an example, the intermolecular and intramolecular hydrogen bonds presented in cellulose were further broken attributed to the incorporation of the sulfonic acid-based BILs in HPW/Si(Et)Si-Dim-SO₃H, which improved the accessibility of hydroxyl groups of cellulose to active sites. Then, the cellulose esterification started from protonation of the carbonyl groups of acetic and propionic anhydride molecules by -SO₃H and HPW active species. During this period, the well-

defined spherical nanostructure can provide large BET surface area with more exposed acid sites, which contributes to improving the accessibility of the reactants with active sites. On the other hand, the inherent strong Brønsted acid nature of as-prepared catalysts ensured the reactions proceed at a considerably fast rate. Later, the protonated carbonyl groups were attacked by the hydroxyl groups of cellulose, and the cellulose ester (CAP) was finally obtained followed by the release of carboxylic acid and proton (Scheme 3). Interestingly, the HPW/Si(Et)Si-Dim-SO₃H-catalyzed cellulose esterification was a controllable process to prevent the depolymerization or degradation of cellulose with the incorporation of HPW and sulfonic acid-based BILs, which is benefit to obtain high value-added CAP products.

Most importantly, the strong Brønsted acidity of as-prepared catalysts was maintained after the reaction due to the strong electrostatic interaction between the anion of HPW and the N⁺ cation of dihydroimidazole and the strong anchoring effect on proton originated from HPW and sulfonic acid-based BILs. Moreover, the loss of proton in as-prepared catalysts could be prevented owing to the acidic reaction system consisted of acetic acid and propionic acid.

Conclusion

To summarize, a series of heterogeneous catalysts by immobilizing HPW and sulfonic acid-based BILs on organosilica nanospheres (HPW/Si(Et)Si-Dim-SO₃H) were successfully fabricated. The heterogeneous catalysts of the spherical HPW/Si(Et)Si-Dim-SO₃H with 7.5% HPW loading showed excellent catalytic activity in the esterification of cellulose to CAP. As a result, the CAP with *DS* of 2.69, viscosity of 447 mPa·s and *M_w* of 102882 was obtained. Such catalytic performance can be assigned to the fact that 1) the well-defined spherical nanostructures provide the large surface area with more exposed acid sites for the HPW/Si(Et)Si-Dim-SO₃H catalyst, which may shorten the mass transfer pathway and thereby improve the accessibility of the reactants with active sites of catalysts; 2) the inherent strong Brønsted acid nature of HPW/Si(Et)Si-Dim-SO₃H by incorporating HPW and sulfonic acid-based BILs is beneficial to obtain high value-added CAP.

Furthermore, the HPW/Si(Et)Si-Dim-SO₃H catalysts showed excellent stability after six consecutive catalytic cycles without obvious loss of catalytic

activity. Therefore, the HPW/Si(Et)Si-Dim-SO₃H can act as efficient and environmentally benign heterogeneous catalysts for the high-value added CAP production.

Acknowledgements

This research was supported by the National Key Research and Development Program of China (2017YFB0307303), the National Nature Science Foundation of China (21625101, 21521005, 21808011), Postdoctoral Science Foundation of China (2018M631313) and the Fundamental Research Funds for the Central Universities (XK1802-6, XK1803-05, XK1902, 12060093063).

References

- Abbott A P, Bell T J, Handa S, Stoddart B (2005) *O*-Acetylation of cellulose and monosaccharides using a zinc based ionic liquid. *Green Chem* 7: 705–707. <https://doi.org/10.1039/B511691K>
- An S, Sun Y, Song D, Zhang Q, Guo Y, Shang Q (2016) Arenesulfonic acid-functionalized alkyl-bridged organosilica hollow nanospheres for selective esterification of glycerol with lauric acid to glycerol mono- and dilaurate. *J Catal* 342: 40–54. <https://doi.org/10.1016/j.jcat.2016.07.004>
- An S, Liu J-C, Zhang H, Wu L, Qi B, Song Y-F (2019) Recent progress on the frontiers of polyoxometalates structures and applications. *Sci China Chem* 62: 159–161. <https://doi.org/10.1007/s11426-018-9378-4>
- Barthel S, Heinze T (2006) Acylation and carbanilation of cellulose in ionic liquids. *Green Chem* 8: 301–306. <https://doi.org/10.1039/B513157J>
- Biganska O, Navard P (2005) Kinetics of precipitation of cellulose from cellulose–NMMO–water solutions. *Biomacromolecules* 6: 1948–1953. <https://doi.org/10.1021/bm040079q>
- Cheng H N, Dowd M K, Shogren R L, Biswas A (2011) Conversion of cotton byproducts to mixed cellulose esters. *Carbohydr Polym* 86: 1130–1136. <https://doi.org/10.1016/j.carbpol.2011.06.002>
- Cao Y, Wu J, Meng T, Zhang J, He J, Li H, Zhang Y (2007) Acetone-soluble cellulose acetates prepared by one-step homogeneous acetylation of cornhusk cellulose in an ionic liquid 1-allyl-3-methylimidazolium chloride (AmimCl). *Carbohydr Polym* 69: 665–672. <https://doi.org/10.1016/j.carbpol.2007.02.001>
- Cao Y, Wu J, Zhang J, Li H, Zhang Y, He J (2009) Room temperature ionic liquids (RTILs): a new and versatile platform for cellulose processing and derivatization. *Chem Eng J* 147: 13–21. <https://doi.org/10.1016/j.cej.2008.11.011>
- Cao Z, Zhao X, He F, Zhou Y, Huang K, Zheng A, Tao D (2018) Highly efficient indirect hydration of olefins to alcohols using superacidic polyoxometalate-based ionic hybrids catalysts. *Ind Eng Chem Res* 57: 6654–6663. <https://doi.org/10.1021/acs.iecr.8b00535>

583 Chen Z, Zhang J, Xiao P, Tian W, Zhang J (2018) Novel thermoplastic cellulose esters containing
 584 bulky moieties and soft segments. *ACS Sustainable Chem Eng* 6: 4931–4939.
 585 <https://doi.org/10.1021/acssuschemeng.7b04466>

586 Edgar K J, Buchanan C M, Debenham J S, Rundquist P A, Seiler B D, Shelton M C, Tindall D
 587 (2001) Advances in cellulose ester performance and application. *Prog Polym Sci* 26:
 588 1605–1688. [https://doi.org/10.1016/S0079-6700\(01\)00027-2](https://doi.org/10.1016/S0079-6700(01)00027-2)

589 El Seoud O A, Marson G A, Ciacco G T, Frollini E (2000) An efficient, one-pot acylation of
 590 cellulose under homogeneous reaction conditions. *Macromol Chem Phys* 201: 882–889.
 591 [https://doi.org/10.1002/\(SICI\)1521-3935\(20000501\)201:8<882::AID-MACP882>3.0.CO;2-I](https://doi.org/10.1002/(SICI)1521-3935(20000501)201:8<882::AID-MACP882>3.0.CO;2-I)

592 Fan G, Wang M, Liao C, Fang T, Li J, Zhou R (2013) Isolation of cellulose from rice straw and its
 593 conversion into cellulose acetate catalyzed by phosphotungstic acid. *Carbohydr Polym* 94:
 594 71–76. <https://doi.org/10.1016/j.carbpol.2013.01.073>

595 Geng Y, Xiong S, Li B, Liao Y, Xiao X, Yang S (2018) H₃PW₁₂O₄₀ grafted on CeO₂: a high-
 596 performance catalyst for the selective catalytic reduction of NO_x with NH₃. *Ind Eng Chem*
 597 *Res* 57: 856–866. <https://doi.org/10.1021/acs.iecr.7b03947>

598 Heinze T, Dicke R, Koschella A, Kull A H, Klohr E, Koch W (2000) Effective preparation of
 599 cellulose derivatives in a new simple cellulose solvent. *Macromol Chem Phys* 201: 627–631.
 600 [https://doi.org/10.1002/\(SICI\)1521-3935\(20000301\)201:6<627::AID-MACP627>3.0.CO;2-Y](https://doi.org/10.1002/(SICI)1521-3935(20000301)201:6<627::AID-MACP627>3.0.CO;2-Y)

601 Heinze T, Liebert T (2001) Unconventional methods in cellulose functionalization. *Prog Polym*
 602 *Sci* 26: 1689–1762. [https://doi.org/10.1016/S0079-6700\(01\)00022-3](https://doi.org/10.1016/S0079-6700(01)00022-3)

603 Hussain M A, Liebert T, Heinze T (2004) Acylation of cellulose with *N,N'*-carbonyldiimidazole-
 604 activated acids in the novel solvent dimethyl sulfoxide/tetrabutylammonium fluoride.
 605 *Macromol Rapid Commun* 25: 916–920. <https://doi.org/10.1002/marc.200300308>

606 Huang K, Wang B, Cao Y, Li H, Wang J, Lin W, Mu C, Liao D (2011) Homogeneous preparation
 607 of cellulose acetate propionate (CAP) and cellulose acetate butyrate (CAB) from sugarcane
 608 bagasse cellulose in ionic liquid. *J Agric Food Chem* 59: 5376–5381.
 609 <https://doi.org/10.1021/jf104881f>

610 Hu J, Wu Q, Li W, Ma L, Su F, Guo Y, Qiu Y (2011) Epoxidation of alkenes catalyzed by phenyl
 611 group-modified, periodic mesoporous organosilica-entrapped, dimeric manganese-salen
 612 complexes. *ChemSusChem* 4: 1813–1822. <https://doi.org/10.1002/cssc.201100382>

613 Inagaki S, Guan S, Fukushima Y, Ohsuna T, Terasaki O (1999) Novel mesoporous materials with
 614 a uniform distribution of organic groups and inorganic oxide in their frameworks. *J Am*
 615 *Chem Soc* 121: 9611–9614. <https://doi.org/10.1021/ja9916658>

616 Inagaki S, Guan S, Ohsuna T, Terasaki O (2002) An ordered mesoporous organosilica hybrid
 617 material with a crystal-like wall structure. *Nature* 416: 304–307.
 618 <https://doi.org/10.1038/416304a>

619 Köhler S, Heinze T (2007) Efficient synthesis of cellulose furoates in 1-*N*-butyl-3-
 620 methylimidazolium chloride. *Cellulose* 14: 489–495. <https://doi.org/10.1007/s10570-007-9138-8>

621
 622 Klemm D, Heublein B, Fink H, Bohn A (2005) Cellulose: fascinating biopolymer and sustainable
 623 raw material. *Angew Chem Int Ed* 44: 3358–3393. <https://doi.org/10.1002/anie.200460587>

624 Kuzminska M, Kovalchuk T V, Backov R, Gaigneaux E M (2014) Immobilizing heteropolyacids
 625 on zirconia-modified silica as catalysts for oleochemistry transesterification and esterification
 626 reactions. *J Catal* 320: 1–8. <https://doi.org/10.1016/j.jcat.2014.09.016>
 627 Kozhevnikov I V, Kloetstra K R, Sinnema A, Zandbergen H W, Vanbekkum H (1996) Study of
 628 catalysts comprising heteropoly acid $\text{H}_3\text{PW}_{12}\text{O}_{40}$ supported on MCM-41 molecular sieve and
 629 amorphous silica. *J Mol Catal A* 114: 287–298. [https://doi.org/10.1016/S1381-1169\(96\)00328-7](https://doi.org/10.1016/S1381-1169(96)00328-7)
 630
 631 Kasztelan S, Payen E, Moffat J B (1990) The existence and stability of the silica-supported 12-
 632 molybdophosphoric acid Keggin unit as shown by Raman, XPS, and ^{31}P NMR spectroscopic
 633 studies. *J Catal* 125: 45–53. [https://doi.org/10.1016/0021-9517\(90\)90076-V](https://doi.org/10.1016/0021-9517(90)90076-V)
 634 Lefebvre F (1992) ^{31}P MAS NMR study of $\text{H}_3\text{PW}_{12}\text{O}_{40}$ supported on silica: formation of
 635 $(\equiv\text{SiOH}_2^+)(\text{H}_2\text{PW}_{12}\text{O}_{40}^-)$. *J Chem Soc Chem Commun* 756–757.
 636 <https://doi.org/10.1039/C39920000756>
 637 Li J, Li D, Xie J, Liu Y, Guo Z, Wang Q, Lyu Y, Zhou Y, Wang J (2016) Pyrazinium
 638 polyoxometalate tetrakaidecahedron-like crystals esterify oleic acid with equimolar methanol
 639 at room temperature. *J Catal* 339: 123–134. <https://doi.org/10.1016/j.jcat.2016.03.036>
 640 Li X, Wang K, Helmer B, Chung T (2012) Thin-film composite membranes and formation
 641 mechanism of thin-film layers on hydrophilic cellulose acetate propionate substrates for
 642 forward osmosis processes. *Ind Eng Chem Res* 51: 10039–10050.
 643 <https://doi.org/10.1021/ie2027052>
 644 Li T, Wang Z, Chen W, Miras H N, Song Y-F (2017) Rational design of a polyoxometalate
 645 intercalated layered double hydroxide: highly efficient catalytic epoxidation of allylic
 646 alcohols under mild and solvent-free conditions. *Chem Eur J* 23: 1069–1077.
 647 <https://doi.org/10.1002/chem.201604180>
 648 Meng C, Cao G, Li X, Yan Y, Zhao E, Hou L, Shi H (2017) Structure of the $\text{SO}_4^{2-}/\text{TiO}_2$ solid acid
 649 catalyst and its catalytic activity in cellulose acetylation. *React Kinet Mech Catal* 121: 719–
 650 734. <https://doi.org/10.1007/s11144-017-1165-3>
 651 Marson G A, El Seoud O A (1999) A novel, efficient procedure for acylation of cellulose under
 652 homogeneous solution conditions. *J Appl Polym Sci* 74: 1355–1360.
 653 [https://doi.org/10.1002/\(SICI\)1097-4628\(19991107\)74:6<1355::AID-APP5>3.0.CO;2-M](https://doi.org/10.1002/(SICI)1097-4628(19991107)74:6<1355::AID-APP5>3.0.CO;2-M)
 654 Omwoma S, Chen W, Tsunashima R, Song Y-F (2014) Recent advances on polyoxometalates
 655 intercalated layered double hydroxides: from synthetic approaches to functional material
 656 applications. *Coord Chem Rev* 258–259: 58–71. <https://doi.org/10.1016/j.ccr.2013.08.039>
 657 Song D, An S, Sun Y, Guo Y (2016) Efficient conversion of levulinic acid or furfuryl alcohol into
 658 alkyl levulinates catalyzed by heteropoly acid and ZrO_2 bifunctionalized organosilica
 659 nanotubes. *J Catal* 333: 184–199. <https://doi.org/10.1016/j.jcat.2015.10.018>
 660 Schnee J, Eggermont A, Gaigneaux E M (2017) Boron nitride: a support for highly active
 661 heteropolyacids in the methanol-to-DME reaction. *ACS Catal* 7: 4011–4017.
 662 <https://doi.org/10.1021/acscatal.7b00808>
 663 Su F, Guo Y (2014) Advancements in solid acid catalysts for biodiesel production. *Green Chem*
 664 16: 2934–2957. <https://doi.org/10.1039/C3GC42333F>

665 Shi Y, Guo Z, Wang Q, Zhang L, Li J, Zhou Y, Wang J (2017) Amphiphilic mesoporous
 666 poly(ionic liquid) immobilized heteropolyanions towards the efficient heterogeneous
 667 epoxidation of alkenes with stoichiometric hydrogen peroxide. *ChemCatChem* 9: 4426–4436.
 668 <https://doi.org/10.1002/cctc.201700906>
 669 Song Y-F, Tsunashima R (2012) Recent advances on polyoxometalate-based molecular and
 670 composite materials. *Chem Soc Rev* 41: 7384–7402. <https://doi.org/10.1039/C2CS35143A>
 671 Tao M, Sun N, Li Y, Tong T, Wieliczko M, Wang S, Wang X (2017) Heteropolyacids embedded
 672 in a lipid bilayer covalently bonded to graphene oxide for the facile one-pot conversion of
 673 glycerol to lactic acid. *J Mater Chem A* 5: 8325–8333. <https://doi.org/10.1039/C7TA01334E>
 674 Tao M, Yi X, Delidovich I, Palkovits R, Shi J, Wang X (2015) Heteropolyacid-catalyzed oxidation
 675 of glycerol into lactic acid under mild base-free conditions. *ChemSusChem* 8: 4195–4201.
 676 <https://doi.org/10.1002/cssc.201501200>
 677 Wu J, Zhang J, Zhang H, He J S, Ren Q, Guo M L (2004) Homogeneous acetylation of cellulose
 678 in a new ionic liquid. *Biomacromolecules* 5: 266–268. <https://doi.org/10.1021/bm034398d>
 679 Xu Q, Song L, Zhang L, Hu G, Chen Q, Liu E, Liu Y, Zheng Q, Xie H, Li N (2018) Synthesis of
 680 cellulose acetate propionate and cellulose acetate butyrate in a CO₂/DBU/DMSO system.
 681 *Cellulose* 25: 205–216. <https://doi.org/10.1007/s10570-017-1539-8>
 682 Yan L, Li W, Qi Z, Liu S (2006) Solvent-free synthesis of cellulose acetate by solid superacid
 683 catalysis. *J Polym Res* 13: 375–378. <https://doi.org/10.1007/s10965-006-9054-x>
 684 Yu Y, Miao J, Jiang Z, Sun H, Zhang L (2016) Cellulose esters synthesized using a
 685 tetrabutylammonium acetate and dimethylsulfoxide solvent system. *Appl Phys A* 122: 656.
 686 <https://doi.org/10.1007/s00339-016-0205-6>
 687 Yan H, Yang Y, Tong D, Xiang X, Hu C (2009) Catalytic conversion of glucose to 5-
 688 hydroxymethylfurfural over SO₄²⁻/ZrO₂ and SO₄²⁻/ZrO₂-Al₂O₃ solid acid catalysts. *Catal*
 689 *Commun* 10: 1558–1563. <https://doi.org/10.1016/j.catcom.2009.04.020>
 690 Zhang Y, Chen X, Li L, Chen W, Miras N H, Song Y-F (2019) Mesoporous polymer loading
 691 heteropolyacid catalysts: one-step strategy to manufacture high value-added cellulose acetate
 692 propionate. *ACS Sustainable Chem Eng* 7: 4975–4982.
 693 <https://doi.org/10.1021/acssuschemeng.8b05627>
 694 Zhu F, Wang W, Li H (2011) Water-medium and solvent-free organic reactions over a
 695 bifunctional catalyst with Au nanoparticles covalently bonded to HS/SO₃H functionalized
 696 periodic mesoporous organosilica. *J Am Chem Soc* 133: 11632–11640.
 697 <https://doi.org/10.1021/ja203450g>
 698 Zhang X, Zhao Y, Xu S, Yang Y, Liu J, Wei Y, Yang Q (2014) Polystyrene sulphonic acid resins
 699 with enhanced acid strength via macromolecular self-assembly within confined nanospace.
 700 *Nature Commun* 5: 3170. <https://doi.org/10.1038/ncomms4170>